EFFECT OF WOOD SPECIES ON THE PORE VOLUME AND SURFACE AREA OF ACTIVATED CARBON DERIVED FROM THE SELF-ACTIVATION PROCESS

Lee M. Smith†
PhD Candidate
E-mail: Leesmith@my.unt.edu

*Sheldon Q. Shi**†
Professor
Department of Mechanical and Energy Engineering
University of North Texas
Denton, TX 76201-76209
E-mail: Sheldonshi@unt.edu

Jiangtao Shi
Associate Professor
College of Materials Science and Engineering
Nanjing Forestry University
Nanjing, China 210037
E-mail: shijt@njfu.edu.cn

Cuicui Wang
Post Doctorate
E-mail: cuicui124@163.com

Yulin Tan
Masters Student
Email: 1195300840@qq.com

Haiying Zhou
PhD Student
Key Laboratory of Bamboo and Rattan Science and Technology of the State Forestry Administration
Department of Bio-materials
International Centre for Bamboo and Rattan
Beijing 100102, China
Email: 15288423522@163.com

(Received November 2019)

Abstract. In this study, the effect of wood species on pore structure of activated carbon (AC) generated from a self-activation process at different dwelling times was investigated. Ten hardwood species were selected (afromosia, alder, black cherry, makore, pomelle sapele, soft maple, teak, walnut, white oak, and yellow poplar) and were activated at 1050°C for three dwelling times (10 h, 5 h, and 2.5 h). X-ray diffraction, Raman spectroscopy, and elemental analysis were performed on AC to analyze the carbon structure. The Brunauer–Emmett–Teller (BET) surface area, Barrett–Joyner–Halenda (BJH) pore volume, and BJH pore width of AC samples were determined. It was shown from the study that the mesopore width of AC decreased as micropores were transitioned to mesopores, leading to an increase in the pore volume and

* Corresponding author
† SWST member

Wood and Fiber Science, 52(2), 2020, pp. 191-207
https://doi.org/10.22382/wfs-2020-017

surface area. The density and porosity of the samples that underwent 2.5-h dwelling time were determined. The porosity of the wood and their resultant AC were compared. The porosity between the wood and its AC possessed a relationship when true and bulk densities of the wood and carbon were compared. The porosity of wood had an impact on the bulk density of the carbon but not on the true density. No relationship was observed between the porosity and surface area of the carbon samples.

Keywords: Activated carbon, wood species, BET surface area, pore volume.

INTRODUCTION

Activated carbon (AC) is a form of graphite that possesses a very dynamic and amorphous surface structure, which combined with the material's pore structure contributes to the material's high surface area (El-Merraoui et al 2000; Xia and Shi 2016a). Because of the surface area and structural properties of AC, it often has various applications, among which water purification and air filtration are the major application areas of AC (Kadirvelu et al 2001; Singh et al 2017). AC is also used as energy material, such as components in both rechargeable batteries and supercapacitors (Gamby et al 2001; Bang et al 2017). Biomass has been a major raw material for AC. Biomass materials include wood (Shi et al 2007), sawdust (Srinivasakannan and Bakar 2004), plant husks (Yalcin and Sevinc 2000), core fibers (Shamasuddin et al 2016), bast fibers, plant shells (Li et al 2008; Chen et al 2016), plant stalks (Hameed et al 2017), and plant waste from various sources (Williams and Reed 2006). The first step for AC fabrication is carbonization. Then, the converted carbon is activated either chemically or physically. When a carbonized material is activated, the pore structure of the carbon expands and the surface area (cm^2/g) increases significantly. The microspore structure of AC is generally most important for its applications (Wigmans 1989), and it is interesting to investigate how the structure of the raw material affects the structure of AC. The shape, size, and distribution of the microspore structure of the raw biomass material can affect the pore structure and surface area of AC. The surface area is usually measured by nitrogen adsorption using the Brunauer–Emmett–Teller (BET) method (Kaneko et al 1992). In fabrication of AC, chemical activation uses chemicals to treat and modify the carbonized material, leading to an increase in the surface area. These can be performed with acids, salts, or bases (Caturla et al 1991). Physical activation, also called thermal activation, uses gases that cause the carbonized material to oxidize, allowing no carbon materials to be removed from the structure through gasification. Carbon dioxide (CO_2) is commonly used as an oxidizer in physical activation. Self-activation uses gases, such as CO_2 produced during carbonization of the biomass, to activate the converted carbon (Shi and Xia 2014; Xia and Shi 2016a, 2016b). One major benefit for the self-activation process is that no activation agents (such as gases and chemicals) are needed for the activation so that the activation cost can be reduced. Because self-activation uses high temperature, major gases generated after activation are mainly carbon monoxide (CO) and hydrogen (H_2) instead of CO_2, which are more environmental friendly.

The application of AC as a material is heavily dependent on its surface area. Through the analysis and comparison of AC rendered from various sources, a better understanding can be gained on how the biomass structure of raw materials affects the activation and structure of the resulted AC. With an improved understanding of material activation, more effective material selection and processing can be achieved when producing the AC for applications. Viability of woods being used to produce AC lies in its pore structure. The pore structure in wood is closely related to the cell type, number, arrangement, and cell wall features of the wood (Rowell 2005). Based on the differences in anatomy, wood is generally divided into softwood and hardwood. Softwoods are mainly composed of more than 90% of tracheid cells; the length of tracheids ranges from less than 3000 μm to 5000 μm, and the diameter is from 10 μm to 35 μm (Richter et al 2004; Meier 2016). There is an obvious difference

Table 1. Wood species information.

Wood species	Wood structure	Density (g/cm^3)	BJH pore width (nm)	
Afromosia (*Pericopsis elata*)	Hardwood/DP	0.725	4.398	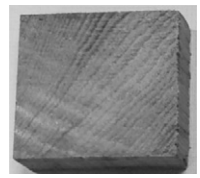
Alder (*Alnus rhombifolia*)	Hardwood/DP	0.45	5.1211	
Black cherry (*Prunus serotine*)	Hardwood/semi-RP	0.56	5.8271	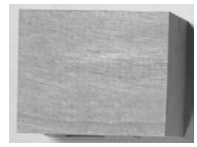
Makore (*Tieghemella heckelii*)	Hardwood/DP	0.685	4.2346	
Pomelle sapele (*Entandrophragma cylindricum*)	Hardwood/DP	0.67	4.4362	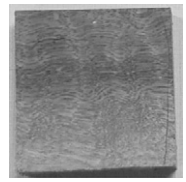
Soft maple (*Acer saccharinum*)	Hardwood/DP	0.53	4.9717	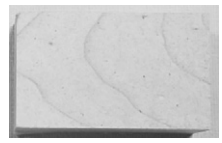
Teak (*Tectona grandis*)	Hardwood/RP	0.74	5.6327	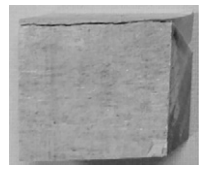
Walnut (*Juglans microcarpa*)	Hardwood/semi-RP	0.64	4.8398	

(continued on following page)

Table 1. Continued.

Wood species	Wood structure	Density (g/cm^3)	BJH pore width (nm)	
White oak (*Quercus alba*)	Hardwood/RP	0.75	4.0469	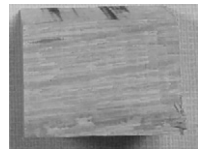
Yellow poplar (*Liriodendron tulipifera*)	Hardwood/DP	0.51	5.0626	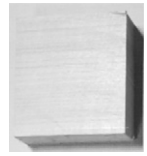

DP, diffuse porous; RP, ring porous.

between the earlywood and latewood in the softwoods but little variation within the wood structure. The density of softwoods is usually between 0.35 g/cm^3 and 0.55 g/cm^3 (Richter et al 2004). Hardwoods, however, have a more complex cellular composition with a large variability in the cell structure. The density of hardwood varies from 0.2 g/cm^3 to 1.2 g/cm^3 (Wheeler et al 1989). Vessels appear across the cross section of hardwoods and possess diameters from one to several hundred micrometers; these vessels are not present in softwoods. Hardwood species are often separated into three categories based on their distribution of vessels: ring porous (RP), diffuse porous, and semi-RP (Meier 2016). This variation in cell components in wood species greatly influences the wood structure and properties. In this study, 10 different hardwood species were selected and compared to establish a relationship in the pore structure between the woods and the derived AC. The effect of activation on the pore structure elements, such as tracheids and vessels, was analyzed. By analyzing the impact of the wood structure on its activation in regard to the pore size and surface area, more efficient material selections can be used when producing AC. The proper material selection can help improve the quality of carbon for specific application and lead to more sustainable resource acquisition and utilization.

MATERIALS AND METHOD

Materials

Samples of 10 hardwood species were selected based on the wood structure and availability, and they were provided by a local wood mill (Table 1).

Measurement of True Accurate Density of Wood

From each wood species, samples with 1 cm^3 were cut, weighed, and measured to determine their volumes. A pycnometer test was performed using a Quantachrome Ultrapyc 1200e pycnometer (Quantachrome, Boynton Beach, FL) to measure the true volume, porosity, open pore, and closed pore value of each sample. Because of the porous nature of wood, the pycnometer was used to test porous wood samples. A pressure of 17 psi was used. The purge mode of the pycnometer was set to "flow," while the run mode was set to "multi." The equilibrium time was 60 s; the maximum run was five, averaged to 3 runs; the run deviation was 0.005%; and the cell size was set to "small." Nitrogen gas was used for the pycnometer test.

Activation Process

A SentroTech STV-1600C-101012 high temperature versatile box furnace (SentroTech,

Strongsville, OH) was used to produce AC from the selected wood samples. The furnace has a chamber size of $10'' \times 10'' \times 12''$, a maximum temperature of 1600°C using $MoSi_2$ heating elements, a maximum pressure of 8 psi, and a maximum ramping rate of 10°C per min.

The furnace was programed with three different activation schedules, where the samples were activated at a temperature of 1050°C and dwelling times of 2.5 h, 5 h, and 10 h, respectively (Fig 1).

Once the activation schedule was programed into the furnace, it was then sealed and pressurized to 720 torr using a vacuum pump. All valves to the furnace were sealed, and the treatment schedule was initiated.

Once the pyrolysis schedule was completed, the furnace was depressurized. The wood samples were removed from the furnace one by one and then had their post pyrolysis mass measured. The initial mass and post pyrolysis mass of each sample were compared to determine the mass loss of each species.

Surface Area Characterization

From each sample, a small piece was cut weighing between 0.05 g and 0.1 g, which was placed inside a testing tube, sealed, and hooked up to a degasser. The samples were then degassed at a temperature of 350°F for a minimum of 1 d. After degassing, the test tubes were then depressurized with nitrogen gas and cooled before they were removed from the degasser. A thermal jacket was placed over the test tubes, and the top of the test tubes was inserted into a foam cap. The test tubes were hooked up to the first and second ports of a Micromeritics 3-Flex surface characterization instrument (Micromeritics, Norcross, GA), and both ports were capable of measuring micro/nanopore structures.

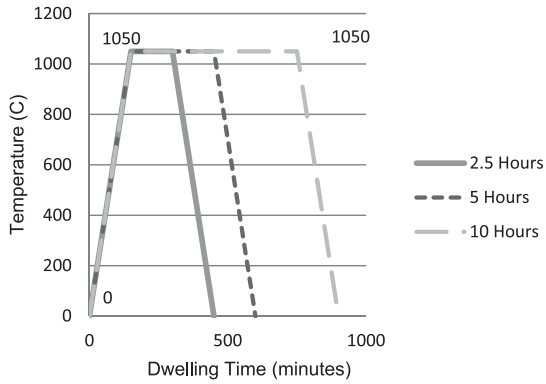

Figure 1. Material activation schedule.

The samples were then degassed by the 3 Flex at a temperature of 350°F for a period of 1,200 min. A thermal mantel attached to the 3 Flex was used to heat the samples at a rate of 2°C/min. After being degassed, the thermal mantel was removed from the test tubes and the thermal jackets on the test tubes were lowered down. An insulated container of liquid nitrogen was placed below the test tubes. The container was lifted up until the test tubes were immersed in liquid nitrogen, at which point surface characterization of the samples inside the test tubes was initiated. Nitrogen gas was pumped in and out of the test tubes, and the absorption and desorption of the samples were measured to determine the surface area and pore size of the samples. This form of characterization recorded the BET surface area, Barrett–Joyner–Halenda (BJH) pore volume, and density functional theory (DFT) measurements of the sample material.

Measurement of True Density of AC

After the samples were weighed after the pyrolysis, a piece of the samples was cut and shaped into a cube as close to the size of approximately 1 cm^3. The length and height were measured using calipers to determine their apparent volumes. The weights of the samples were measured to determine their apparent density. The samples then underwent a pycnometer test using a Quantachrome Ultrapyc 1200e pycnometer. The pycnometer was set to a pressure of 6 psi, purge mode of "flow," equilibrium time of 180 s, run mode of "multi," with a maximum run of 5, averaged to 3 runs, with a run deviation of 0.005%. The cell size used for the sample was in microscale. The difference between the pycnometer test of the wood samples and that of the

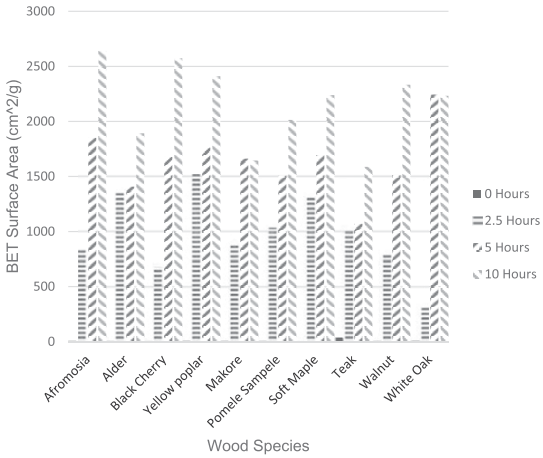

Figure 2. BET surface area of wood species as a function of dwelling time.

AC samples was due to the highly porous nature of the AC compared with that of the wood; the AC samples were tested at a much lower pressure for a longer equilibrium time to allow for a more accurate reading. Cells of the same size were used for all the samples. For the wood samples, the pycnometer was calibrated with a small calibration sphere, while for the AC samples, microspheres were used to calibrate the pycnometer. After the test was performed, the porosity, true volume, and the true density of the samples were determined.

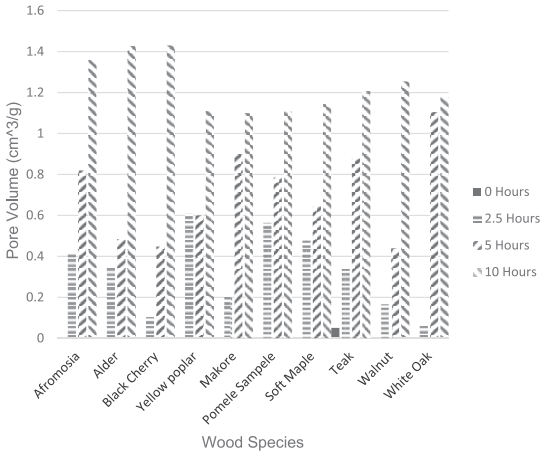

Figure 3. BJH pore volume of wood species as a function of dwelling time.

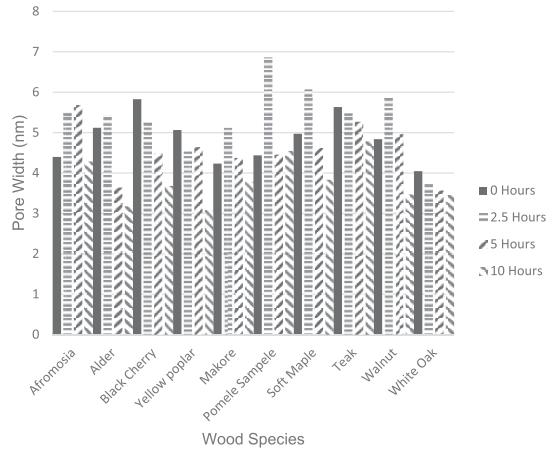

Figure 4. BJH pore width of wood species as a function of dwelling time.

Elemental Analyzer Preparation and Procedure

A Sundy SDCHN435 Carbon Hydrogen & Nitrogen Analyzer (Hunan Sundy Science and Technology Development Co., Ltd., Changsha City, Hunan, China) was used to determine the elemental contents of carbon, hydrogen, and nitrogen of the wood species and their AC. The AC samples were ground to powder using a mortar and pestle, after which 75.0 g to 100 g of AC was placed within an aluminum foil cup and sealed within it to remove as much oxygen as possible from the carbon. The samples were then loaded into the analyzer, where they underwent destructive testing in accordance with the procedure described in ASTM D5373-08. The carbon and hydrogen contents were measured using IR absorption, and the nitrogen content was determined using thermal conductivity detection as the carbon samples were burnt from the test.

Raman Spectroscopy Testing Parameters

Raman spectroscopy was performed on the wood species AC to determine the level of graphitization that had occurred on the surface structure by comparing the level of disorder that is present between the defective structures present in the diamond band (I_D) and the crystalline structure present in the graphite band (I_G). By looking at

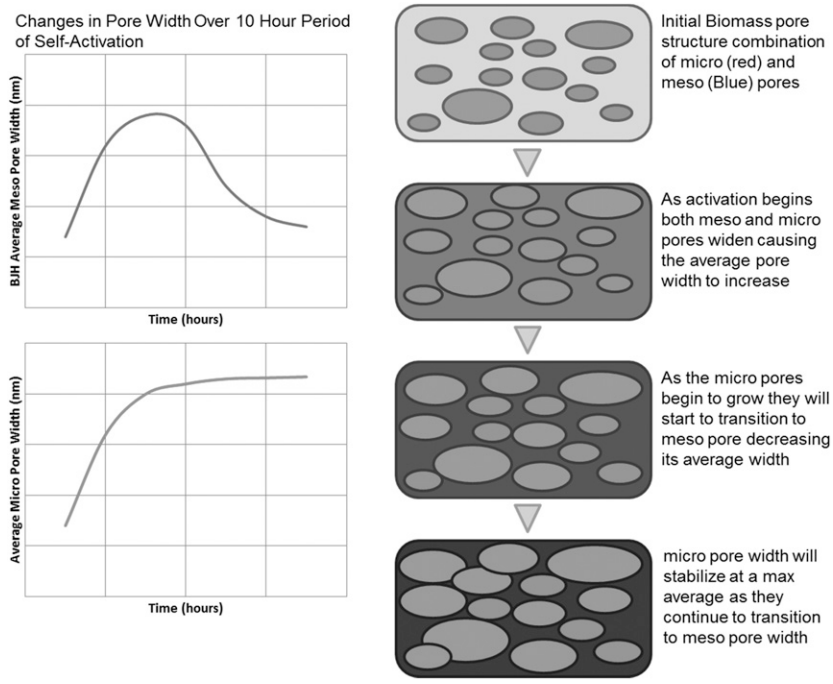

Figure 5. Changes in pore width throughout self-activation.

this comparison, the level of breakdown of the carbon structure can be understood. A HORIBA Scientific LabRAM HR Evolution Raman spectrometer (Horiba Scientific, Kyoto, Japan) was used to analyze the wood species AC after it had been ground using a mortar and pestle. The AC samples were placed onto a glass slide and brought into focus under 50× magnification, after which magnification was increased to 100× magnification, where an optimal spot to perform Raman spectroscopy was selected. Raman spectroscopy was performed using LabSpec 6 software (Horiba Scientific, Kyoto, Japan) with an acquisition time of 10 s, laser with a 532-nm edge, a grating of 300 (600 nm), and a wavelength scan range from 1000 cm^{-1} to 2000 cm^{-1}. This range was selected to observe the presence of the diamond band (D-band) and graphite band (g-band) of the carbon. The I_G/I_D value of the AC was determined by dividing the intensity of the g-band (I_G) by the intensity of the D-band (I_D), which can be used to determine surface graphitization. The I_G/I_D value can be used to determine the quality of the electrical conductivity of the AC, which is useful when considering end application.

X-Ray Diffraction (XRD) Testing Parameters

XRD was performed on the powder made from the wood AC using a PHILIPS X'Pert (Philips, Amersterdam, The Netherlands) to analyze the defect in graphene layers present in the carbon as dwelling time was increased. A continuous scan was performed with a scan range of 5-80 2θ, a step size of 0.1 2θ, using a 2.00-mm fixed divergent slit, a tube current of 40 A, and a generator voltage of 40 V. The powdered AC samples were placed on a glass sample holder and mounted within the XRD. An empirical value (R) was used to calculate the ratio of the peaks (002) and (101) to help characterize the structure of the carbon (Liu et al 1995).

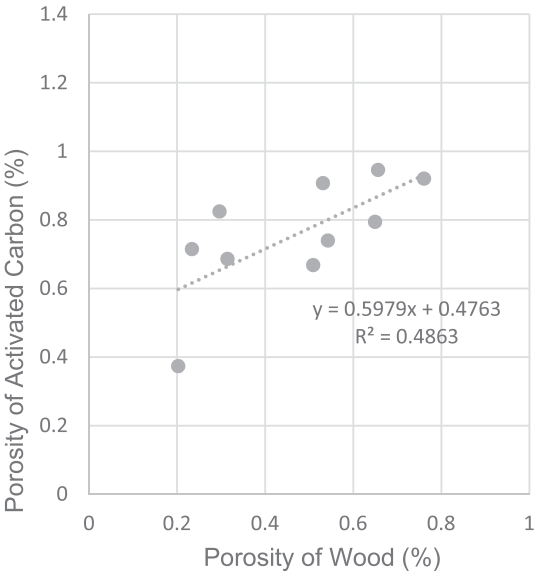

Figure 6. Porosity of wood vs porosity of activated carbon (2.5 h at 1050°C).

RESULTS AND DISCUSSION

Effect of Dwelling Time on the Pore Structure and Surface Properties

The BET values were used to compare the changes in the surface area of the hardwood species and their AC at different dwelling times (Fig 2). It was observed that as the dwelling time increased, the surface area increased for the wood species as well (Fig 3). However, the difference in the BET surface area at different dwelling times differed with species. For the alder and teak AC, the surface area increased slightly from 2.5 h to 5 h dwelling time. By contrast, the surface area of makore and white oak increased slightly from 5 h to 10 h dwelling time. This showed that each wood species would reach different surface areas at different thermal activation times.

A similar trend was observed for the pore volume data of the wood and carbon structure (Fig 3). Overall, the pore volume of all wood carbon increased as the dwelling time increased. However, different increments were observed with different activated times for each wood species. As shown in Fig 3, the pore volume of yellow poplar carbon activated at 2.5 h and 5 h is similar. The pore volume of makore and white oak increased dramatically from 2.5 h to 5 h. Significant increases in pore volume for alder, black cherry, and walnut were observed from 5 h to 10 h. These results indicated that the activation behaviors depended on the different wood species.

It was observed from the changes in the BJH average pore width of the wood species and their carbon that as the dwelling time increased, there was an initial peak in the pore width followed by its decrease (Fig 4). Xia and Shi (2016b) recorded that as the dwelling time increased, the DFT micropore-specific surface area increased in the initial first 10 h then began to decrease, whereas the BJH mesopore-specific surface area only increased up to the 100-h maximum dwelling time. When compared with Xia and Shi (2016b)'s study, the hardwood properties were only characterized to a maximum of 10-h

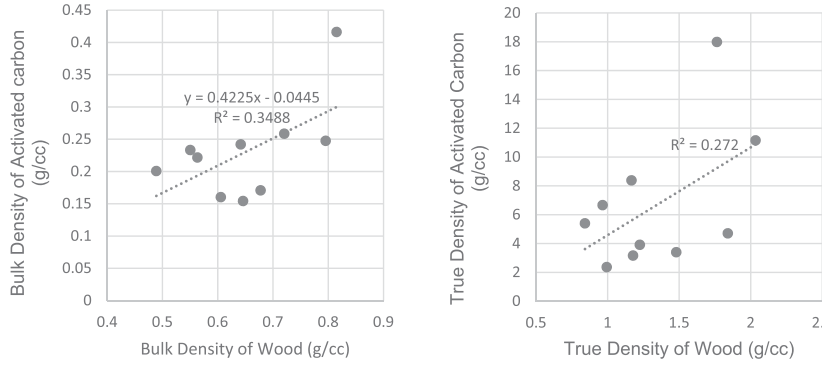

Figure 7. (a) Bulk density of wood species vs bulk density of activated carbon (AC) and (b) true density of wood species vs true density of AC.

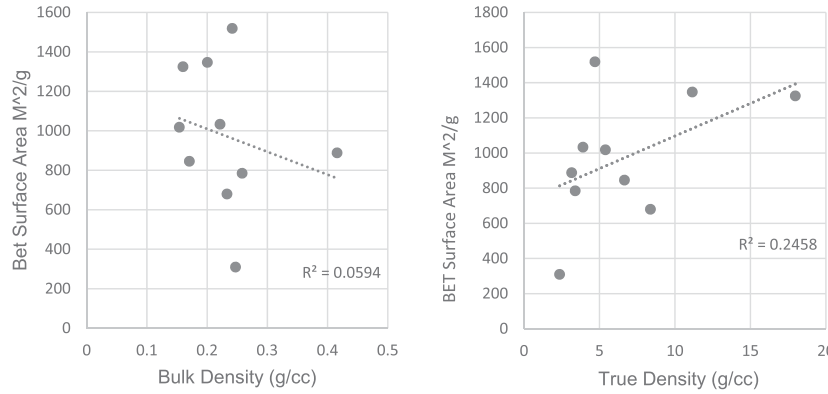

Figure 8. (a) Bulk density vs BET surface area of activated carbon (AC) (2 0.5 h at 1050 C) and (b) true density vs BET surface area of AC (2.5 h at 1050 C).

dwelling time. The decrease in the DFT-specific surface area in Xia and Shi (2016b) took place during the same time as the fluctuation of the BJH mesopore width of the hardwood species took place. For both this work and the work described in Xia and Shi (2016b), only the BJH mesopore-specific surface area increased as the dwelling time increased. This indicated that as the dwelling time increased, the average BJH mesopore width was impacted by the changes in the micropore structure. Therefore, as the dwelling time increased, the micropore structure increased and then transitioned to the mesopore structure (Fig 5).

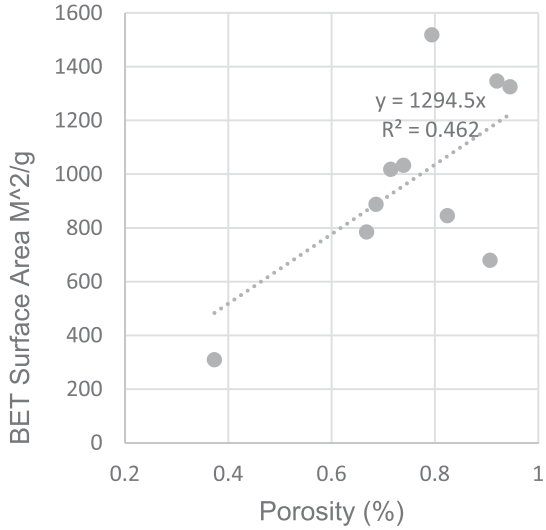

Figure 9. Porosity vs BET surface area of activated carbon (2.5 h at 1050 C).

The transition of micropores to mesopores caused a decrease in the mesopore width after the initial peak and over time. As the dwelling time increased, the number of micropores that transitioned to mesopores decreased, causing the average pore width to increase at higher dwelling time. However, not all wood species showed the similar changing pattern on the pore width with the activation time. For example, the width of black cherry, teak, white oak, and yellow poplar pore decreased at 2.5-h dwelling time, indicating that the initial peak of these species would occur at an earlier time during activation.

These changes in the pore width were based on the wood cell types and arrangement of the cells, which were dependent on the wood species. As the wood structure underwent initial activation, the average pore width increased for both meso- and micropores, and as the cell structure underwent gasification, the average pore width began to decrease for micropores. As the dwelling time increased and the initial removal of material from the pore structure occurred, the average mesopore width began to decrease as the micropores transitioned to mesopores. This would indicate that as the initial pore width expanded during carbonization, an increase in the volume and surface area of the pore structure happened, which led to the transitioning of micro- to mesopores, where the pores began to interconnect, causing the surface area and pore volume to increase to higher values.

Because hardwoods mainly consist of different proportions of vessels, fiber cells, rays, and

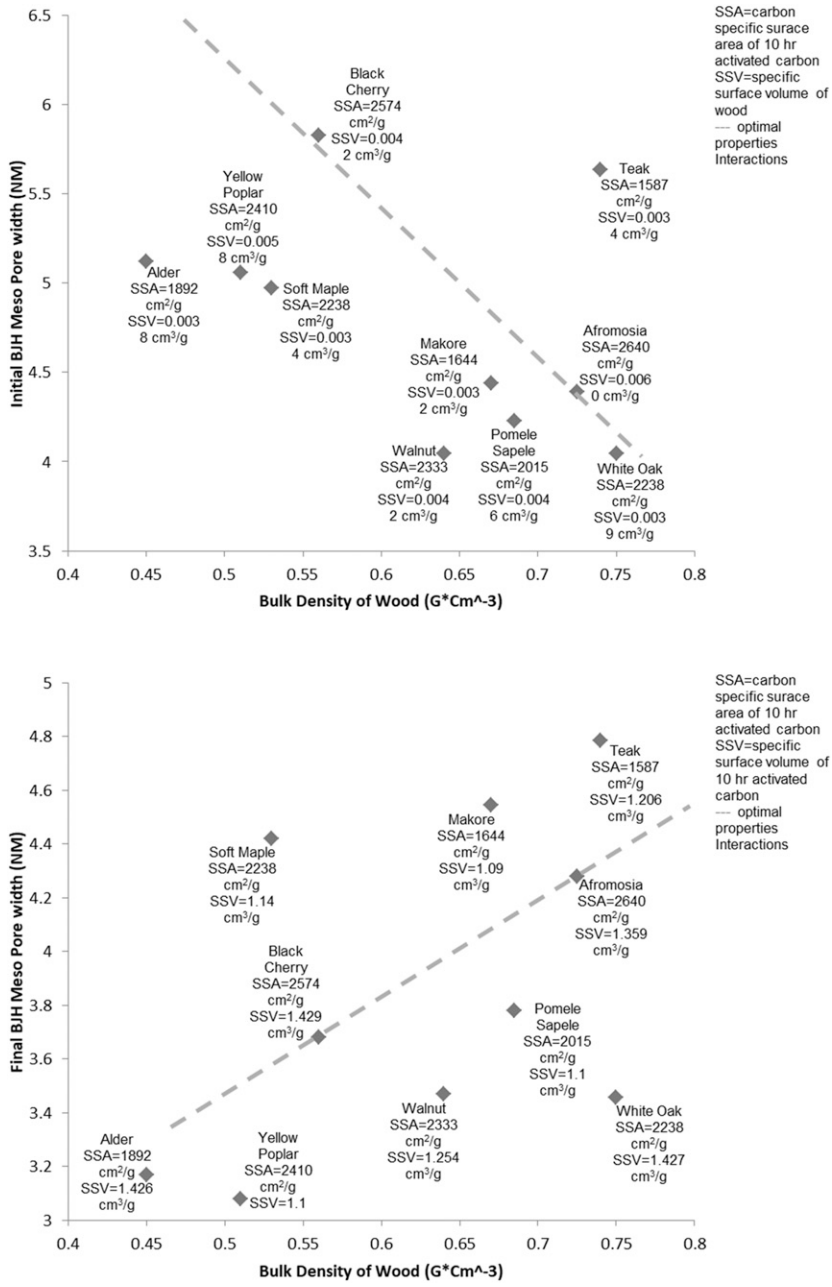

Figure 10. (a) Bulk density of wood vs BJH pore width of wood and (b) bulk density of wood vs BJH pore width of 10 h activated carbon.

parenchyma cells, these wood cells make up 35-45% of the wood substance. When a longer dwelling time was used, these vessels and parenchyma cells collapsed quite easily.

Porosity Analysis

By performing a pycnometer test on both the hardwood and the AC derived from them, true

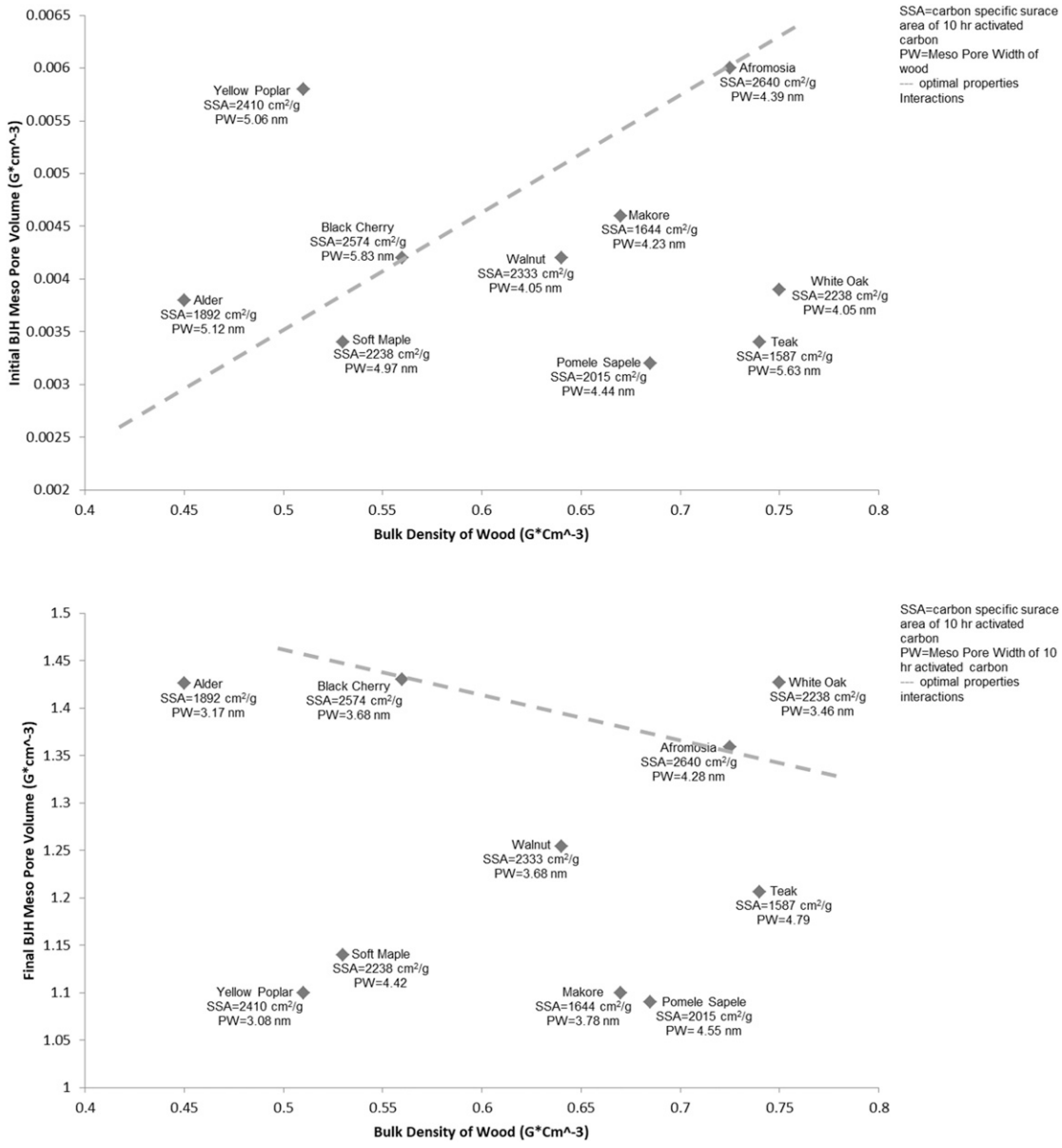

Figure 11. (a) Bulk density of wood vs BJH pore volume of wood and (b) bulk density of wood vs BJH pore volume of 10 h activated carbon.

volumes of the samples were determined. The AC that underwent a 2.5-h dwelling time was used in the comparison. The bulk density and bulk volume were used to determine the true density and the porosity of the samples. A positive upward trend was observed between the porosity of the wood and the porosity of the resulted AC (Fig 6), indicating that the porosity of the wood could impact the porosity of its AC.

Both bulk and true densities of the wood and the resulted AC were characterized. As shown in Fig 7, for both density measurements, correlations

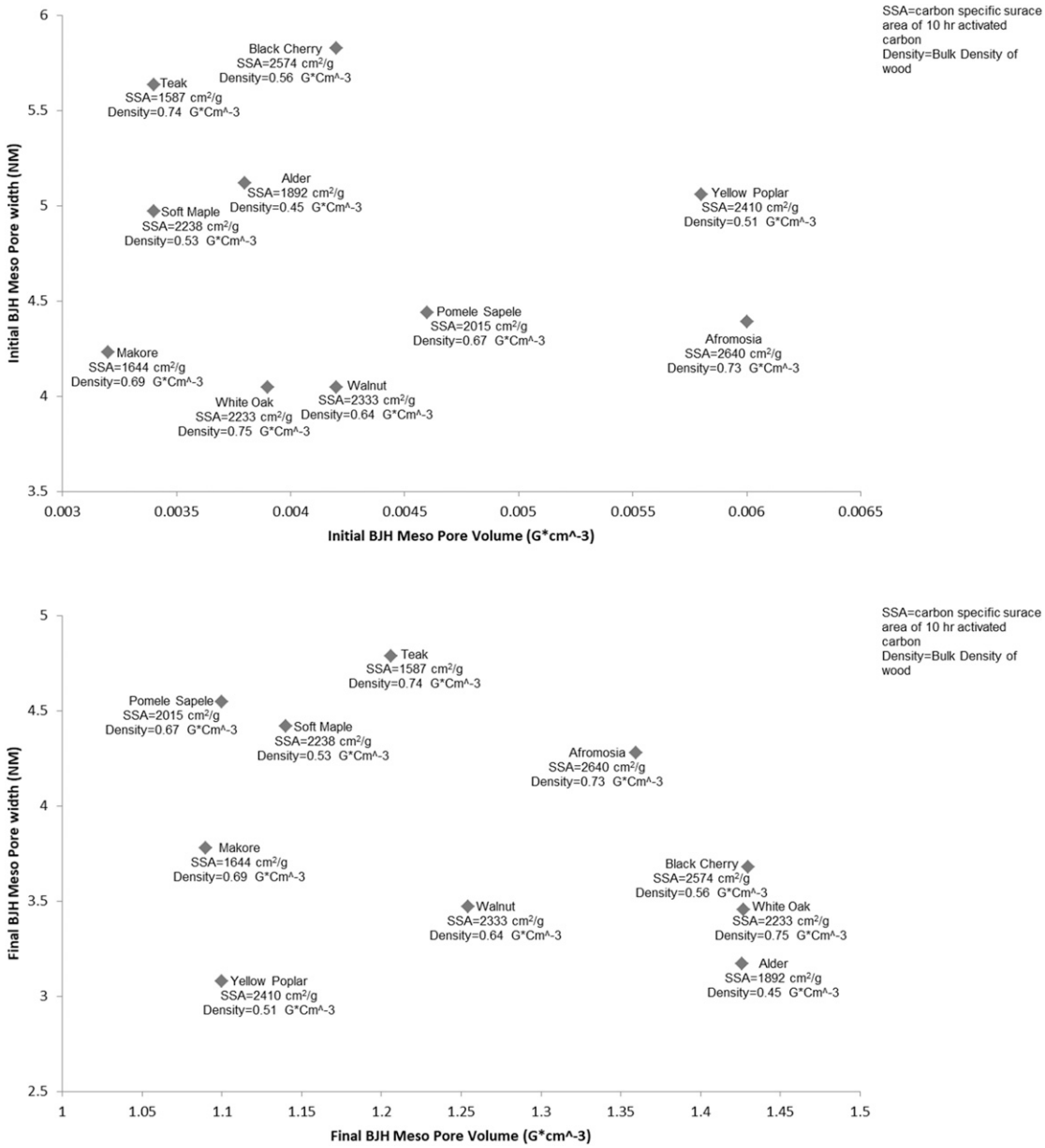

Figure 12. (a) BJH pore volume vs BJH pore width of wood and (b) BJH pore volume of 10 h activated carbon vs BJH pore width of 10 h activated carbon.

between the wood and the resulted AC were shown, while the correlation between the bulk densities was stronger. The bulk density measurement of a material includes its porosity, taking into account the material's pore structure. The true density measurement does not measure the pore volume. Therefore, the difference between the bulk and true density showed that a material's pore structure had an impact on its activation (Fig 7[a] and [b]).

Both bulk and true densities of the AC were compared against the BET surface areas among

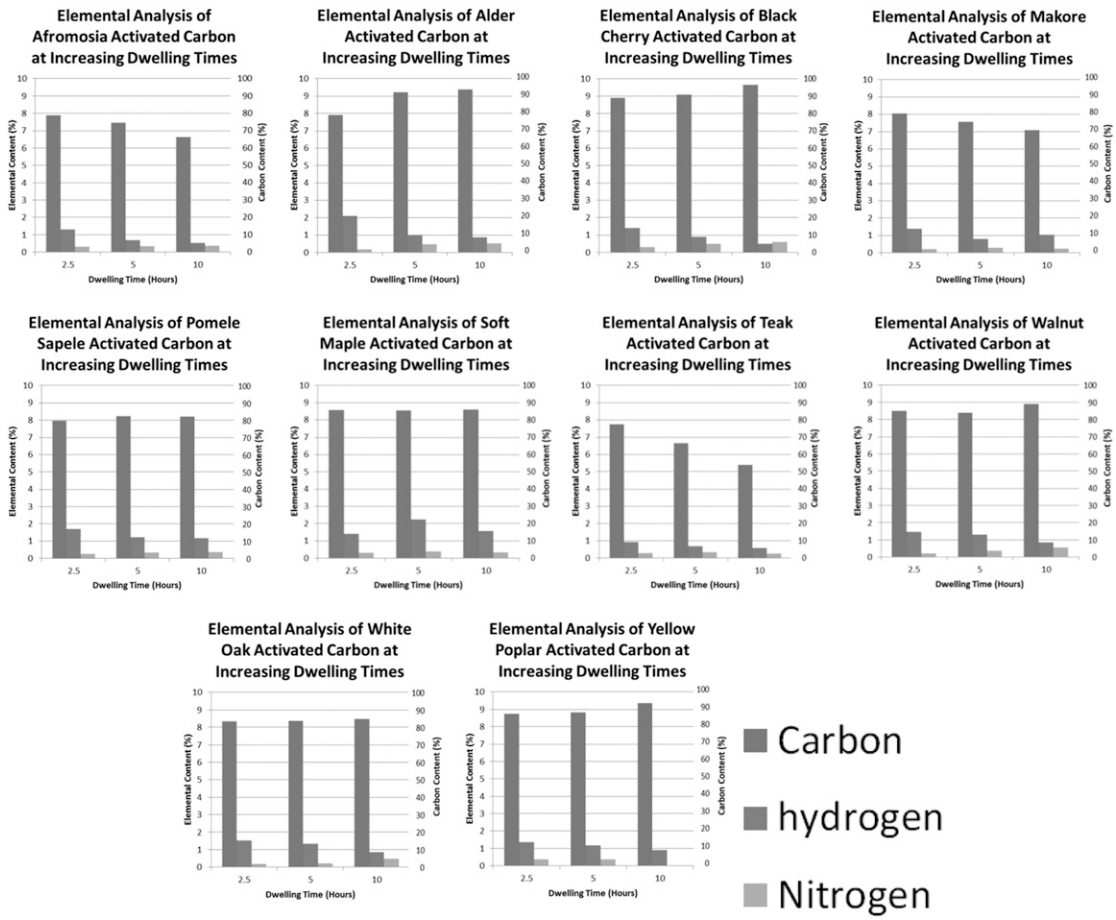

Figure 13. Elemental analysis of each wood species as dwelling time increases.

the wood species (Fig 8). As shown in Fig 8, the true density of the AC had a closer relationship with the surface area than the bulk density, indicating that the relationship between the density and surface area did not correspond to the relationship between the porosity and surface area (Figs 8[a] and [b] and 9). It was seen that the density did not have a relationship with the surface area of the carbon. The bulk density measurements of the hardwood species were plotted against the BJH mesopore width and against the BJH mesopore volume (Figs 10-12). The analysis of the surface properties of these species showed that wood species with a low bulk density, low volume, and large pore width or a high bulk density, high volume, and small pore width possessed a high BET surface area. By comparing the other wood species with those that performed the best, it could be determined that based on their changes in the pore width (Fig 4), changes to the activation schedule would be needed to improve their surface properties. The reason that bulk density was used for this comparison was that bulk density as a measurement included the porosity of the structure, and porosity did present a relationship between wood and its AC (Fig 6). Therefore, bulk density could be a suitable indicator of a wood species structure. By subjecting these 10 hardwood species to the same activation conditions, an idea of the optimal ratio of structural properties was seen in the two species of afromosia and black cherry,

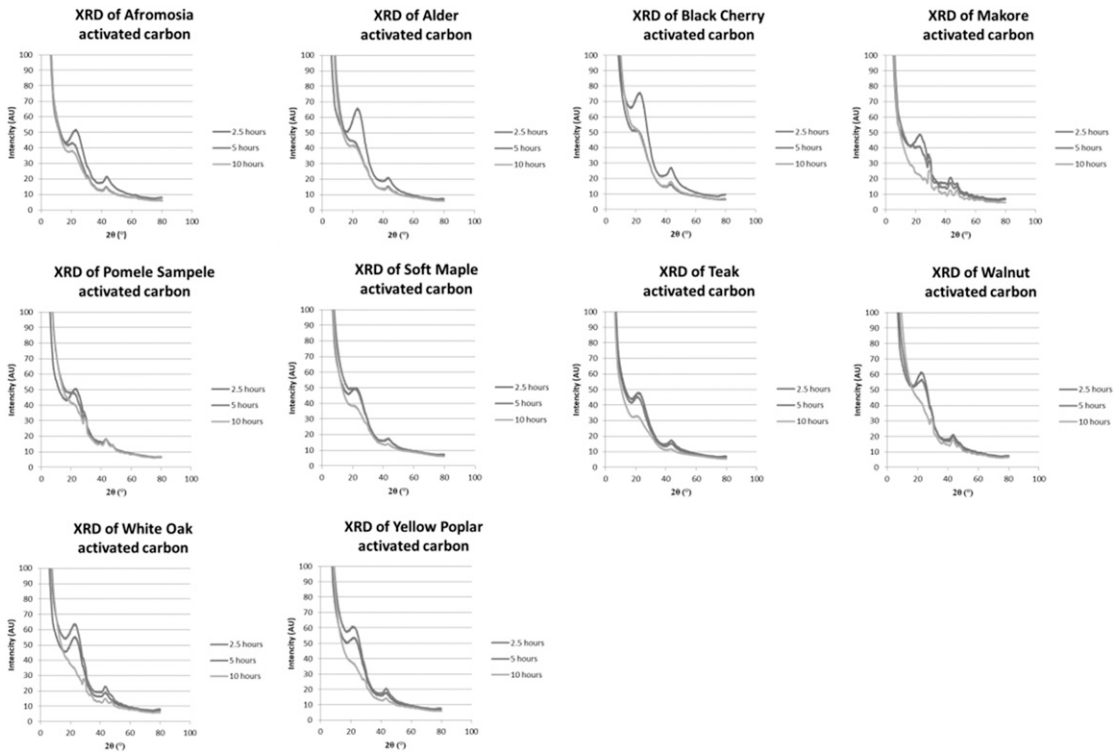

Figure 14. X-ray diffraction (XRD) of activated carbon.

with which the other wood species could be compared to determine exactly what changes to the activation parameters would be needed to improve their final surface area. Teak used in this study possessed a high bulk density, but its pore width and pore volume were much different from the other high bulk density woods. Therefore, it could be determined that teak would need a longer activation time to further improve its surface area.

Effect of Dwelling Time on Elemental Composition and Structure

As the wood undergoes activation and is rendered to AC, the pore structure is degraded as gasified and activated. The elemental composition changes throughout self-activation because of the removal of material, which results in a carbon structure. The hardwood species AC was characterized using XRD, Raman spectroscopy, and elemental analysis to understand the changes in the elemental content and structure as the dwelling time increases.

It was observed that as the dwelling time increased, the bulk density of the carbon decreased. From the

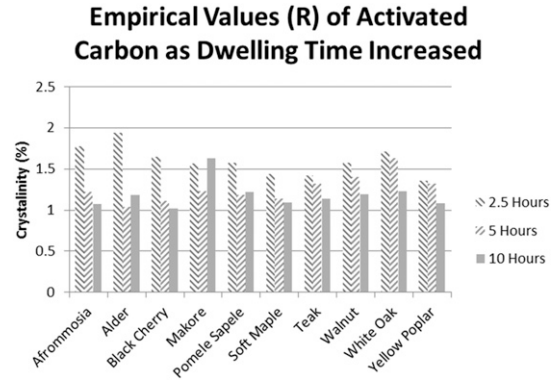

Figure 15. Empirical values of activated carbon as dwelling time increases.

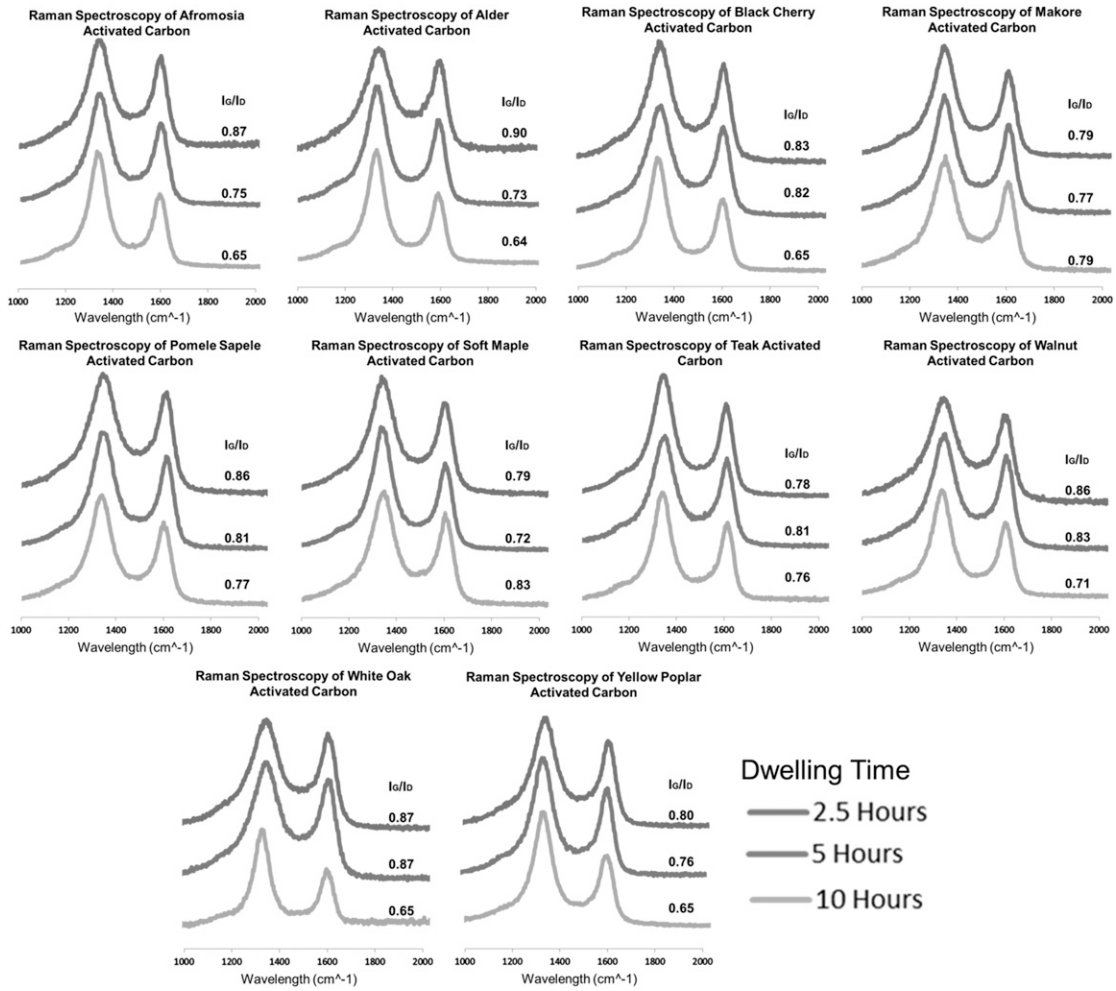

Figure 16. Raman spectroscopy of activated carbon.

results of the elemental analysis, as the dwelling time increased, the amount of the material needed and the volume of the material increased. This presented problems for some samples whose volume was too high to meet the minimum mass, which impacted their final results at the 10-h dwelling time. It was observed that for most of the samples, the content of carbon increased as the dwelling time increased, whereas for teak, afromosia, and makore, the carbon content decreased (Fig 13). The measurement of the carbon content was based on the elemental analysis of AC by combusting the samples. For species with a high inorganic content, the actual carbon content would be decreased with activation. Teak, afromosia, and makore are known for having a high silicon content (Meier 2016), which would be the reason for their reduced carbon content.

The contents of hydrogen and nitrogen were much less in the AC than that of the carbon, and these contents were reduced overall for the species as the dwelling time increased. It was observed that as the dwelling time increased to 10 h, the density of yellow poplar was too low, and the analyzer was unable to provide an accurate reading on the nitrogen content. The changes of the elemental content in the different

AC samples showed the impact of the dwelling time on fiber structure degradation.

The XRD analysis of the AC showed a decrease in the intensity of the peaks around 2θ values of 23° and 43°, which corresponded to the (002) and (101) planes (Brommier et al 2015) and represented the structural properties of the graphene layers that made up the carbon (Fig 14). It was observed that the *R* values decreased as the dwelling time increased, indicating the increase in the disorder of the structure (Fig 15). Xia et al (2016) attributed the increase in disorder to the complexity of the surface structure as it underwent longer activation, which caused even greater degradation to the AC. This disorder could be contributed to faults, interspacing, or strain in between the graphene layers Girgis et al (2007).

From Raman spectroscopy testing of the AC, it could be seen that the D-band of the carbon occurred around a wavelength of 1330 cm^{-1} and the G-band occurred around 1590 cm^{-1} (Fig 16). The calculated I_G/I_D value of the AC of the different wood species varied, showing how they reacted to changes in dwelling time. Xia et al (2016) observed an increase in the I_G/I_D value in pine wood. However, in this study, the maximum time observed was 32 h, which would see a large amount of modification to the surface structure due to activation. Because of the fact that each of the hardwood ACs were only treated for 10 h, the variation between each species could be contributed to differences in the structural properties of each wood.

By looking at the elemental composition of the structure, the impact of the dwelling time was shown on the AC. As the dwelling time increased, the disorder of the carbon structure increased, and more elements in the structure were removed. This removal also showed how complex the pore structure was due to the disorder in the graphene layers of the carbon, which contributed to the increase in surface properties.

CONCLUSIONS

To understand the relationship between wood species, pore structure, and activation parameter impact of the AC rendered from the wood, the ACs were fabricated through a self-activation process at different dwelling times on 10 hardwood species. The surface properties of the AC sample derived from these species were characterized to evaluate how the material activation affected the pore structure of ACs. The following conclusions can be drawn:

1. As the dwelling time increased, the surface area and pore volume of the AC increased. However, as the dwelling time increased, the BJH average mesopore width initially increased then decreased, indicating that at a certain point of activation, the width of micropores began to transition into mesopores. Therefore, the change in the pore width could serve as an indicator of the state of activation of the biomass.
2. Positive relationships were presented between the porosity of the wood and its carbon, and between the porosity and surface area.
3. No specific relationship was found between the pore width and pore volume of the raw material on its AC. There was no trend present between the bulk density and pore width, and between the bulk density and pore volume. From the characterization of the 10 hardwood species, an interaction between the bulk density, pore width, and pore volume was found. By comparing the surface properties of the carbons with the results of black cherry and afromosia, which had the highest surface properties, optimal property interactions were observed. This information can be used to determine optimal activation conditions based on surface properties of the wood.
4. The results of XRD, Raman spectroscopy, and elemental analysis of the carbon showed that as the dwelling time increased, the carbon content of the samples increased, except for teak, afromosia, and makore. The complexity of the carbon graphite structure increased as the dwelling time increased because of the increased levels of disorder between the graphene layers, as they were broken and degraded from activation. However, graphitization of carbon surfaces from different species varied.

ACKNOWLEDGMENTS

The work was supported by the USDA Foundation Program Grant# 12213597. Special thanks to the International Center for Bamboo and Rattan in Beijing, China, for the help with some characterizations.

REFERENCES

Bang JH, Lee HM, An KH, Kim BJ (2017) A study on optimal proe development of modified commercial activated carbons for elecrode materials of supercapacitors. Appl Surf Sci 415:61-66.

Brommier C, Xu R, Wang W, Wen D, Lu J, Ji X (2015) Self-activation of cellulose: A new preparation methodology for activated carbon electrodes in electrochemical capacitors. Nano Energy 13:709-717.

Caturla F, Molina-Sabio M, Rodriguez-Reinoso F (1991) Preparation of activated carbon by chemical activation with $ZnCl_2$. Carbon 29(7):999-1007.

Chen D, Chen X, Sun J, Zheng Z, Fu K (2016) Pyrolysis polygeneration of pine nut shell: Quality of pyrolysis products and study on the preparation of activated carbon from biochar. Bioresour Technol 216:629-636.

El-Merraoui M, Aoshima M, Kaneko K (2000) Micropore size distribution of activated carbon fiber using the density functional theory and other methods. Langmuir 16(9): 4300-4304.

Gamby J, Taberna P, Simon P, Faubarque J, Chesneau M (2001) Studies and characterization of various activated carbons used for carbon/carbon supercapacitors. J Power Sources 101(1):109-116.

Girgis B, Temerk Y, Gadelrab M, Abdullah I (2007) X-ray diffraction patterns of activated carbons prepared under various conditions. Carbon Lett 8(2):95-100.

Hameed B, Din A, Ahmad A (2007) Adsorption of methylene blue onto bamboo-based activated carbon: Kinetics and equilibrium studies. J Hazard Mater 3(22):819-825.

Kadirvelu K, Thmaraiselvi K, Namasivayam C (2001) Removal of heavy metals from industrial wastewaters by adsorption onto activated carbon prepared from an agricultural solid waste. Bioresour Technol 76(1):63-65.

Kaneko K, Ishii C, Ruike M, Kuwabara H (1992) Origin of super high surface area and microcrystalline graphitic structures of activated carbons. Carbon 30(7):1075-1088.

Li W, Yang K, Peng J, Libo Z, Guo S, Xia H (2008) Effects of carbonization temperatures on characteristics of porosity in coconut shell chars and activated carbons derived from carbonized coconut shell chars. Ind Crops Prod 28(2):190-198.

Liu Y, Xue JS, Zheng T, Dahn JR (1995) Mechanism of lithium insertion in hard carbons prepared by pyrolysis of epoxy resins. Carbon 34(2):193-200.

Meier E (2016) WOOD! Identifying and using hundreds of woods worldwide. The Wood Database.

Richter HG, Grosser D, Heinz I, Gasson PE (2004) IAWA list of microscopic features for softwood identification. IAWA J 25(1):1-70.

Rowell RM (2005) Handbook of wood chemistry and wood composites. CRC Press, Boca Raton, FL.

Shamasuddin M, Yusoff N, Sulaiman M (2016) Synthesis and characterization of activated carbon produced from kenaf core fiber using H_3PO_4 activation. Procedia Chem 19:558-565.

Shi SQ, Xia C (2014) Porositization process of carbon or carbonaceous materials. U.S. Patent 14/211,357, 18 9 2014.

Shi Y, Chrusciel L, Zoulalian A (2007) Production of charcoal from different wood species. *In* Recents progres en genie des procedes. Paris, France.

Singh G, Kim IY, Lakhi KS, Srivastava P, Naidu R, Vinu A (2017) Single step synthesis of activated bio-carbons with a high surface area and their excellent CO_2 adsorption capacity. Carbon 116:448-455.

Srinivasakannan C, Bakar MZA (2004) Production of activated carbon from rubber wood sawdust. Biomass Bioenergy 27(1):89-96.

Wheeler EA, Baas P, Gasson PE (1989) IAWA list of microscopic features for hardwood identification. IAWA J 10(3):219-332.

Wigmans T (1989) Industrial aspects of production and use of activated carbon. Carbon 89(1):13-22.

Williams PT, Reed AR (2006) Development of activated carbon pore structure via physical and chemical activation of biomass fibre waste. Biomass Bioenergy 30(2): 144-152.

Xia C, Shi SQ (2016a) Self-activation process to fabricate activated carbon from kenaf. Wood Fiber Sci 48:62-69.

Xia C, Shi SQ (2016b) Self-activation for activated carbon from biomass: Theory and parameters. Green Chem 18(7): 2063-2071.

Xia C, Kang C, Mumukshu PD, Cai L, Gwalani B, Banerjee R, Shi SQ, Choi W (2016) Pine wood extracteedactivated carbon through self-activation process for high-performance lithium-ion battery. Chem Sel 1(13):4000-4007.

Yalcin N, Sevinc V (2000) Studies of the surface area and porosity of activated carbons. Carbon 38(14):1943-1945.